RESEARCH ARTICLE

Macromolecular Materials and Engineering
Open Access
www.mame-journal.de

Material Testing for Physicists: Unraveling the Dissipative Nature of Silicone Elastomers via Ball Drop Testing

Rene Preuer, Carina Emminger, Umut Cakmak, and Ingrid Graz**

Isaac Newton once contemplated the fall of an apple, setting in motion a revolution in the understanding of gravity. In a similar spirit of curiosity and inquiry, here a journey is embarked upon to explore the intricate world of viscoelastic damping for polydimethylsiloxanes (PDMS). Inspired by the notion that even the simplest of phenomena can yield profound insights, a novel approach to study damping in silicone elastomers through a simple ball drop test is introduced. This novel solution allowes for precise measuring and analyzing the material's damping characteristics under various conditions. By carefully controlling the release and monitoring, the response of the falling ball by simple video tracking, valuable insights into the key viscoelastic properties of silicone blends are extracted, including rebound resilience, Young's modulus, and complex modulus. Through the analysis of trajectory data generated during the sphere's interaction with the silicone damper, dynamic and static material parameters are determined. Remarkably, these outcomes closely align with results obtained from cost-intensive and high-maintenance industrial measurement setups such as dynamic thermomechanical analysis (DTMA) or tensile testing. This approach not only simplifies the complexity of the system but also offers a cost-effective and efficient means of gaining essential knowledge in material science.

1. Introduction

Newton is famous for his observation of an apple falling from a tree—we took inspiration and studied a bouncing ball and derived a tool for physicist to characterize soft materials. Bouncing balls are well known[1] and demonstrate nearly any facet of elementary mechanics including viscoelastic nature of rubbers, allowing it to slowly dissipate energy upon repeated impact. Physicists can now take a lesson from this playful use of material science. Initiated by Newton's laws, an experimental approach of dropping a hard sphere onto a soft elastic solid is adopted and subsequently exploited for rebound resilience. Revisiting Hertz theory on contact,[2,3] the reduced modulus for derivation of the Young's modulus is extracted allowing the characterization of modern-day silicone elastomers polydimethylsiloxanes (PDMS). PDMS[4] represents the omnipresent soft platform of novel evolutions of electronics,[5,6] optics,[7] and robotics in research labs worldwide.[8,9] Their easy processability by means of mold-casting as well as their readily miscibility often require an on-the-spot characterization. However, this characterization often solely comprises cost-efficient classical tensile tests simply extracting Young's modulus,[10] while more thorough dynamic thermomechanical analysis (DTMA) requires expensive equipment.[11] Only very few approaches to simplify or reduce cost of testing equipment are undertaken by custom-designed tensile/compression testers.[11–14] In addition to the simple mechanical characterization for extracting the Young's modulus using tensile tests, silicone elastomers are also known for their inherently dissipative properties due to their macromolecular crosslinked network structure with a multitude of applications in medical, power, consumer, automotive, and aerospace applications.[15] While frequency-dependent energy dissipation can be evaluated by means of DTMA, there are often only qualitative tests using a ball drop setup.[16] In such a ball drop test, the impact of a ball and subsequent rebound is recorded allowing us to compare materials damping properties. We have taken this simple concept of a ball drop further to enable cheap and simple material characterization.

Our research highlights the practicality and significance of utilizing the ball drop test as a method to deduce material parameters associated with damping in silicone elastomer blends,[17] with a specific focus on off-the-shelf PDMS materials Sylgard 184

R. Preuer, I. Graz
Christian Doppler Laboratory for Soft Structures for Vibration Isolation and Impact Protection (ADAPT)
School of Education
STEM Education
Johannes Kepler University Linz
Altenbergerstrasse 69, Linz 4040, Austria
E-mail: rene.preuer@jku.at; ingrid.graz@jku.at
C. Emminger, U. Cakmak
Christian Doppler Laboratory for Soft Structures for Vibration Isolation and Impact Protection (ADAPT)
Institute of Polymer Product Engineering
Johannes Kepler University Linz
Altenbergerstrasse 69, Linz 4040, Austria

The ORCID identification number(s) for the author(s) of this article can be found under https://doi.org/10.1002/mame.202400085

DOI: 10.1002/mame.202400085

(Dow Corning) and Ecoflex 00–30 (Smooth-On). The prime aim here is on using these silicone elastomers for impact protection and tailor their damping properties. By creating blends of both silicones under various mixing conditions, the tuneability of the respective damping properties is explored by means of an impact test as a key method. Hereby, a steel ball is released from a fixed height to free fall and impacts onto an elastomeric damping element. The trajectory of the ball is recorded through high-speed video tracking. This approach enables the correlation of the interaction between the sphere and the soft substrate and the resulting deformation with both the stress–strain relationship obtained from tensile tests and the material's damping capacity assessed through the loss tangent (also known as loss factor (tanδ)) in DTMA measurements. Through this comprehensive approach, various material parameters are indirectly determined by the governing equations of a bouncing ball.[18] By using the governing equation of this kinematic problem, we can extract static properties such as Young's modulus and dynamic characteristics like storage modulus, loss modulus, and the loss tangent. Furthermore, our methodology provides insights into the damping attributes of the material, including parameters such as rebound resilience and the energy dissipated during impact. The ball drop test, owing to its practicality, cost-effectiveness, and straightforward implementation, offers a promising approach for gaining a comprehensive understanding of elastomer material properties for soft robotics, in general, but for impact protection applications, in particular.

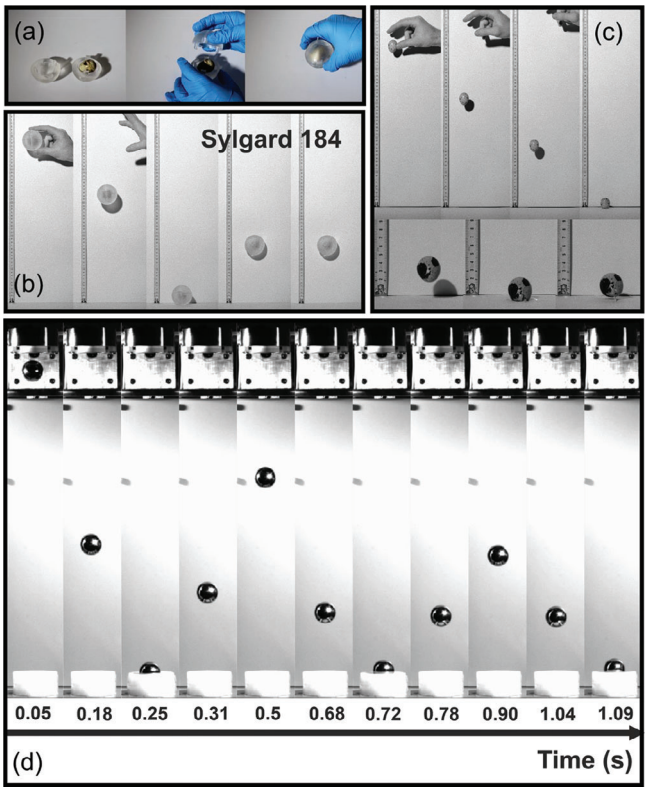

Figure 1. a) Concept of protective casing for a quail's egg made from silicone and b) evaluation of damping properties in a drop test. c) Comparison with unprotected egg inspiring d) the ball drop experiment.

2. Results and Discussion

We started exploring the damping properties of silicone elastomers by means of designing ball shaped casings (with a diameter of 6 cm and a wall thickness of 1 cm) made from PDMS (Sylgard 184 and Ecoflex 00–30) for enclosing a quail's egg (**Figure 1**a). The PDMS ball was then subjected to a drop test (Figure 1b), where it was dropped from a fixed height of 45 cm, and the drop and impact were recorded by means of a high-speed camera. After the ball drop the integrity of the egg was evaluated showing that either silicone material offers sufficient damping to protect the egg versus when no casing is used (Figure 1c).

Intrigued by the simplicity of such a ball drop and the curiosity to explore PDMS material properties in more detail, we designed our ball drop experiment for simplicity, cost efficiency, and minimal maintenance. It comprises an aluminum frame to ensure a consistent drop height, an electromagnet for controlled ball release, a ruler for postprocessing video analysis reference, and a high-speed camera for recording videos at a high-frame rate. By means of this setup, steel balls of various diameters (1–4 cm) are dropped from various heights (25, 45, and 65 cm) onto cylindrical silicone elastomer blend samples with a radius of 3 cm and a height of 2 cm. Upon release, the ball drop and impact upon the samples are tracked using a high-speed camera (Phantom v711-8G-M, Vision Research) at a rate of 1600 fps, allowing for precise monitoring of the entire impact sequence (Figure 1d).

The elastomer blend samples were prepared by combining Sylgard 184 and the much softer Ecoflex 00–30. By varying the mixing ratio between the two off-the-shelf silicones, Sylgard 184 and Ecoflex 00–30, we have the precise ability to fine-tune the blend material's mechanical properties,[19] in general, and its response upon impact, in particular. This enables us to custom-tailor the damping characteristics to meet our specific requirements, as illustrated in **Figure 2**a. The blending process is straightforward, with Sylgard 184 (denoted as E0) and Ecoflex 00–30 (denoted as E100) processed separately according to the manufacturers' specifications (10:1 for Sylgard 184 and 1:1 for Ecoflex 00–30). They were then blended together in 10% ratio increments per weight (with the respective ratios denoted as E*X*, where *X* is the weight ratio percentage of Ecoflex 00–30 in the blend). Detailed steps for fabricating these silicone elastomer blends can be found in the "Experimental Section." For temperature-dependent measurements, the blend test specimens were preconditioned for 2 h in an environmental chamber, maintaining temperatures between −50 and +50 °C.

Upon release, the ball drop and impact upon the samples were tracked using a high-speed camera (at a rate of 1600 fps, allowing for precise monitoring of the entire impact sequence (see Figure 2b). Visualizing rebound height provides insights into the effect of blending on damping capacity. Subsequently, video footage underwent postprocessing with tracking software (Tracker Version 6, Physlets) to provide essential data regarding the ball's trajectory, including displacement, velocity, and acceleration during and after the impact exemplarily shown for a 3 cm ball onto Sylgard 184 (refer to Figure 2c,d). Recording at a high frame rate lets us closely observe the impact event, spanning from the initial contact of the ball with the testing specimen to their subsequent separation. This process provides data on

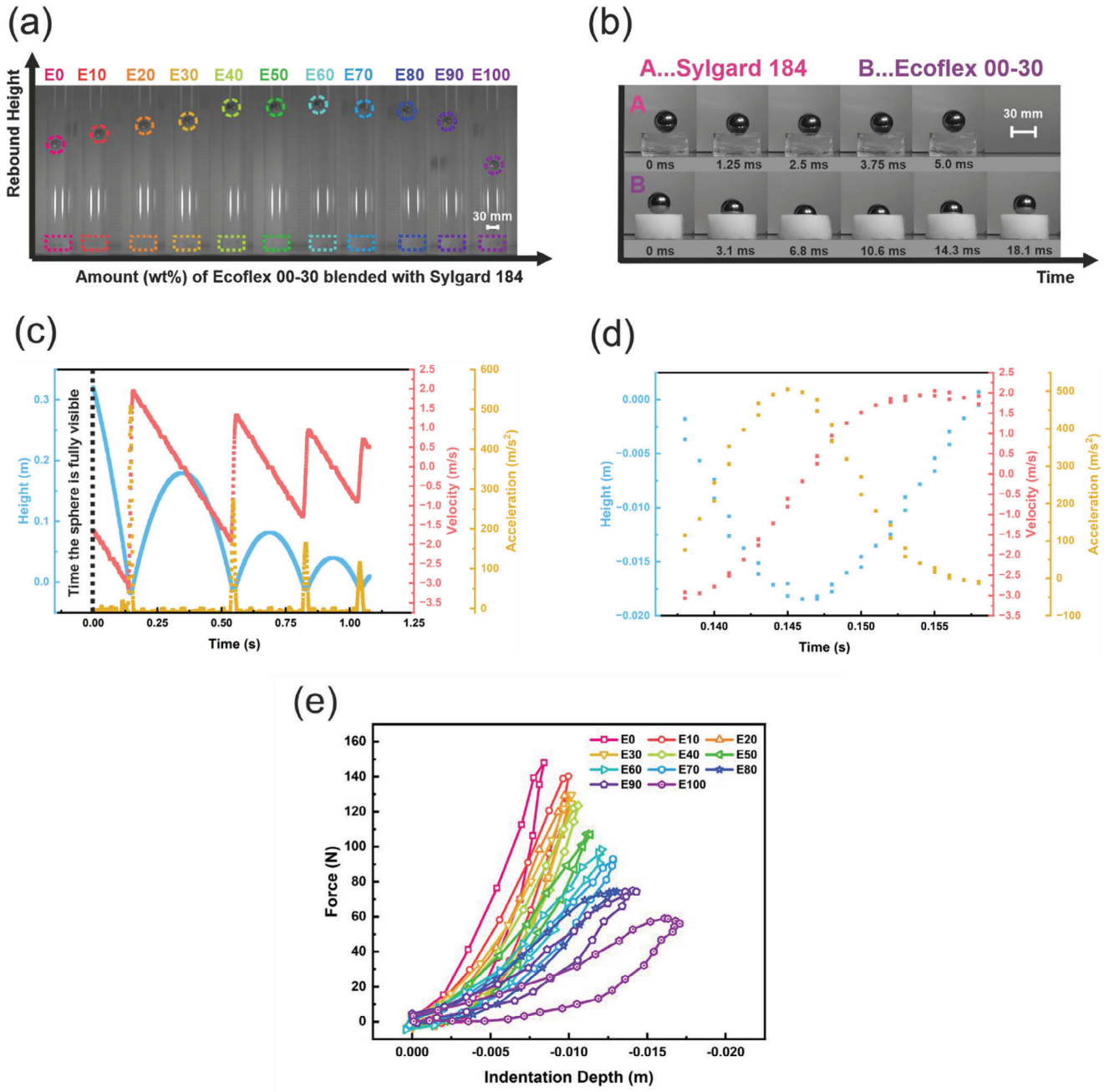

Figure 2. a) Rebound heights after impacting elastomer specimens ranging from pure Sylgard 184 (E0) to 100% Ecoflex 00-30 (E100), illustrating the effect of blending on damping capacity. b) Image sequence depicting a 3 cm ball dropped from 45 cm onto pure Ecoflex 00–30 and Sylgard 184 at 30 °C, highlighting contact times of ≈18 ms for Ecoflex 00–30 and 5 ms for Sylgard 184. c) Graph derived from video displaying displacement, velocity, and acceleration data during the ball's descent and rebound on Sylgard 184, indicating energy dissipation through trajectory reduction, analyzed from video recordings. d) Tracking data of the ball's first impact on Sylgard 184, detailing indentation depth, maximum acceleration, and dissipation through velocity change. e) Load–displacement curves resulting from ball indentation into the blends at 30 °C, depicting energy dissipation by the area enclosed in the hysteresis loop.

indentation depth, maximum acceleration, and velocity changes for the calculation of energy dissipation during the event (see Figure 2d).

Utilizing information regarding the ball's mass (1 cm: 4 g; 2 cm: 32 g; 3 cm: 109 g; and 4 cm: 258 g), allows for deriving the indentation force generated by the ball as well as potential and kinetic energy throughout both the descent and rebound stages. Plotting force–displacement data during the contact phase yields hysteresis curves that exhibit variations with distinct mixing ratios, as depicted in Figure 2e. These curves (conditions: drop height = 45 cm, T = 30 °C, 3 cm ball) offer valuable insights into the energy dissipation per unit volume of the material per stress

cycle.[20] The cyclic integral of force with respect to displacement, graphically represented by the area enclosed within the hysteresis loop, quantifies the work done against the damping force during the contact time. This integral, often referred to as the loop area, signifies the energy dissipated during each cycle of motion.

For the sake of comparative analysis, we computed the energy dissipation through the determination of potential and kinetic energy differences before and after the impact, documented in **Table 1**. The dataset uncovers the exceptional damping characteristics of the off-the-shelf materials, with Ecoflex 00–30 (denoted as E100) emerging as the most efficient damping material in our comparison, with Sylgard 184 (denoted as E0) coming in second. However, as the concentration of Ecoflex 00–30 within the blends increases, the damping properties exhibit a gradual decline, reaching a minimum at a 60% weight ratio (E60) of Ecoflex 00–30. At this juncture, the damping capability is nearly half that of pure Ecoflex 00–30. Subsequently, a further increase in the content of Ecoflex 00–30 results in an improvement of damping properties.

Intriguingly, these findings are in contrast to the silicone elastomer blends haptic properties. They are gradually getting softer as the amount of Ecoflex 00–30 increases, a phenomenon that seemingly contradicts the observed dissipative characteristics. This finding is in robust agreement with the DTMA data (Figure S1, Supporting Information) clearly highlighting that damping is not simply related to stiffness. While stiffness depends on the elasticity of the bonds between the atoms/molecules which make up the spring, the damping depends on the permanent distortion of the bonds which are not (simply) related. While Ecoflex and Sylgard are built up from the same base PDMS,[19] they differ in their molecular weight, crosslinking density, and fillers, resulting in particular complex formulation for the blends and subsequent inherent morphological characteristics that cannot easily be determined. In our quest to delve deeper into material properties, we drew inspiration from indentation principles for hardness measurements. This involves lowering a small testing tip (<4 mm in diameter) onto a specimen, gradually deforming it, while monitoring both the indentation load P and the displacement h throughout a full loading and unloading cycle. This enables the measurement of stress and strain relations akin to the force–displacement curves witnessed during the ball's impact onto the soft damper. This inspired us to extend our investigation further, with the aim of unraveling critical information about the material's stiffness, a property conventionally referred to as Young's Modulus by applying the indentation method proposed by Oliver and Pharr.[21,22] By analyzing the load–displacement data, we can derive the reduced modulus, a parameter linked to Young's modulus through Equation (1)[21]

$$\frac{1}{E_r} = \frac{\left(1-\nu^2\right)}{E} + \frac{\left(1-\nu_i{}^2\right)}{E_i} \tag{1}$$

where E_r represents the reduced modulus, while E and ν represent the Young's modulus and Poisson's ratio for the elastomer blend. E_i and ν_i denote the same parameters for the steel ball acting as the indenter.

The calculation of the reduced modulus involves determining the slope in the upper segment of the unloading cycle, as

Table 1. Analyzed energy dissipation during initial impact by calculating the hysteresis loop area and the difference in potential and kinetic energy before and after impact. A 3 cm diameter ball was dropped from 45 cm onto test specimens at 30 °C.

Dissipated energy [J]	Blends E0–E100	E0	E10	E20	E30	E40	E50	E60	E70	E80	E90	E100
Hysteresis		0.232	0.22	0.182	0.178	0.145	0.140	0.133	0.135	0.145	0.158	0.274
Potential energy difference		0.225 ± 0.003	0.192 ± 0.006	0.171 ± 0.008	0.157 ± 0.005	0.125 ± 0.005	0.123 ± 0.004	0.109 ± 0.001	0.121 ± 0.004	0.129 ± 0.005	0.163 ± 0.009	0.283 ± 0.003
Kinetic energy difference		0.237 ± 0.003	0.206± 0.003	0.17 ± 0.008	0.155 ± 0.001	0.123 ± 0.003	0.119 ± 0.0003	0.116 ± 0.002	0.123 ± 0.003	0.131 ± 0.005	0.161± 0.003	0.284 ± 0.001

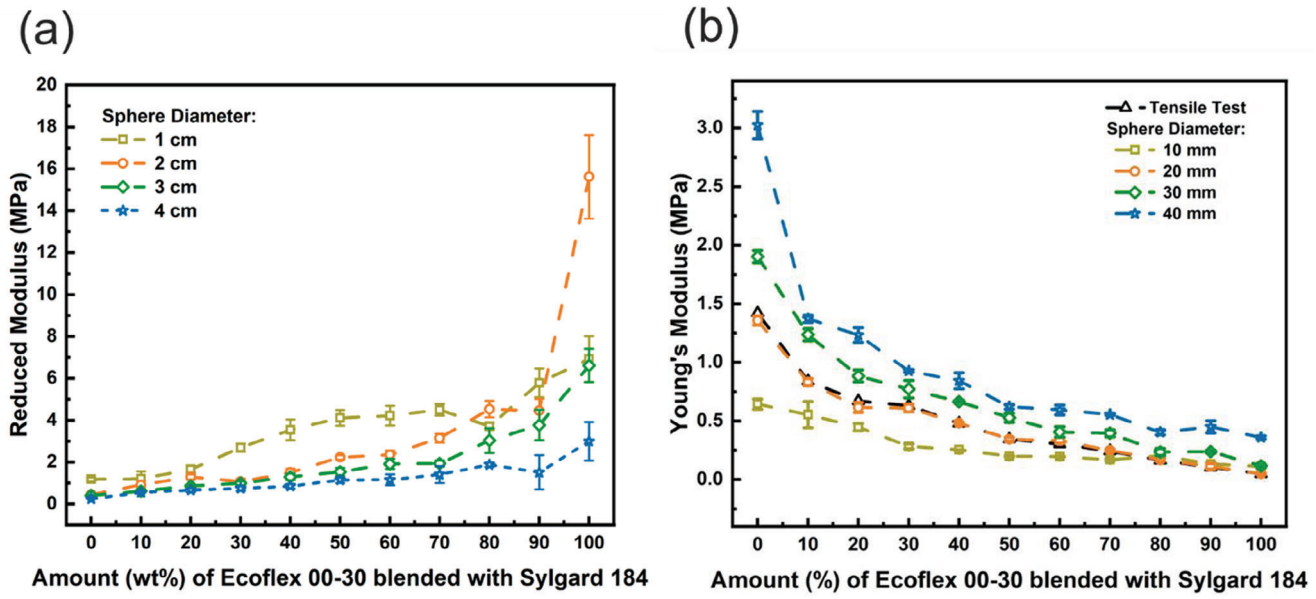

Figure 3. a) The reduced modulus for spheres with radii ranging from 1 to 4 cm was investigated. These spheres were dropped from a height of 45 cm onto testing specimens at 30 °C. The determination of the reduced modulus involved calculating the slope in the upper segment of the unloading cycle and assessing the contact area based on the maximum indentation depth. b) Calculated Young's modulus values for sphere radii ranging from 1 to 4 cm, dropped from a height of 45 cm onto the elastomer testing specimens at 30 °C. The dashed line represents the Young's modulus obtained from tensile tests conducted at a rate of 1 mm s^{-1}.

described in Equation (2)

$$S = \frac{dP}{dh} = \frac{2}{\sqrt{\pi}} E_r \sqrt{A} \tag{2}$$

where S, denoted as dP/dh, is the ratio between indentation load P and the displacement h, and signifies the experimentally measured stiffness from the unloading data, and A represents the contact area of the sphere at maximum indentation, as calculated in Equation (3)

$$A = 2\pi r h_{max} \tag{3}$$

Here r stands for the radius of the ball, and h_{max} represents the maximum indentation depth, obtained from tracking data.

By calculating the slope and contact area from the force–displacement curves of the ball drop test and applying them to Equation (2), we are able to determine the reduced modulus (**Figure 3a**). By inserting the reduced modulus into Equation (1), while taking into account the Young's modulus of the stainless steel ball at 205 GPa[23] and its Poisson's ratio at 0.30,[24] along with the Poisson's ratio of the elastomer blends at 0.495,[25] we determine the corresponding Young's moduli for the blends across sphere radii ranging from 1 to 4 cm, as depicted in Figure 3b, respectively. The latter graph depicts the calculated elastic modulus for sphere diameters ranging from 1 to 4 cm, dropped from a height of 45 cm onto the elastomer blends at 30 °C. Additionally, we conducted a tensile test to validate the calculated theoretical data with the Young's modulus derived from stress–strain curves. For comprehensive details on the tensile test results, please refer to Figure S2 (Supporting Information). For comprehensive comparison with the calculated values, see Table S1 (Supporting Information).

Our analysis reveals a good agreement with the Young's modulus values obtained via tensile tests, in particular for the 2 cm diameter ball. Similarly, data for the 1 cm ball allow for extracting the elastic modulus for data specimens with higher Ecoflex 00–30 content (<70 wt%) (E70). Test with larger ball diameters (3 and 4 cm) reveal less agreement. In general, deviations are more significant for the lowest and highest amounts of Ecoflex 00–30 for reduced modulus and Young's modulus, respectively. Overall, this approach using the force–displacement curves works best for softer materials (such as Ecoflex 00–30 with a shore 00 of 23 as compared to Sylgard 184 with shore A of 38 and 00 of 80[19]) due to the larger number of data points during contact time. Further, we also learn that indentation testing via a ball drop experiment strongly relies on the ratio of the sphere's contact area to the specimen's dimensions,[26,27] revealing that the testing balls require to be of smaller diameter than the sample height and radius of 3 cm, respectively.

The ball drop tests for extracting the force–displacement curves are considered as dynamic events, where each ball impact results in the dissipation of energy. As the sphere descends onto the test specimen, as illustrated in **Figure 4a**, its gravitational potential energy $E_{pot} = (mgh_{drop})$ transforms into kinetic energy ($E_{kin} = 1/2\ mv^2_{drop}$), and vice versa, post impact. When contact occurs, the sphere initiates deformation in the specimen, leading to a gradual reduction in the sphere's velocity, ultimately bringing it to a complete stop. During this process, a portion of the sphere's initial kinetic energy is transformed into elastic strain energy, which is stored within the material, while the remainder is dissipated by internal viscosity.[28] Subsequently, as the specimen returns to its initial state, utilizing the

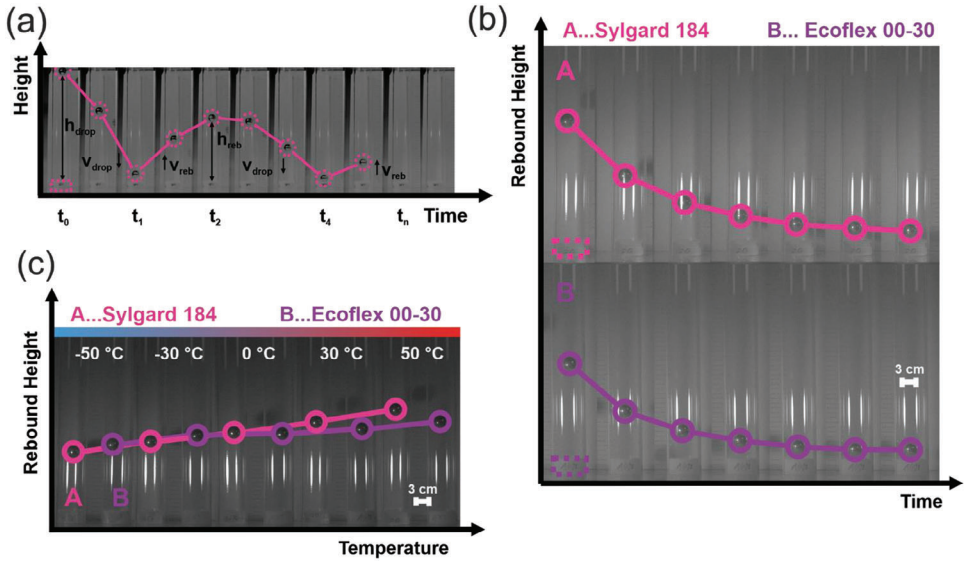

Figure 4. a) Schematic of the energy dynamic during fall and subsequent rebounds of the ball. b) Initial and subsequent rebound heights of the ball on both Sylgard 184 (E0) (top) and Ecoflex 00–30 (E100) (bottom) for a drop height of 45 cm, revealing a subsequent decrease in stored energy. c) Rebound heights after impact at temperatures between −50 and 50 °C.

remaining energy that has not dissipated, it propels the sphere upward.

The sphere rebounds with a lower velocity v_{reb} than its initial preimpact velocity v_{drop} resulting in a reduced rebound height h_{reb} (see Figure 4b). This energy transformation allows us to calculate the rebound resilience, a crucial parameter indicating the material's ability to recover and restore kinetic energy following deformation, providing valuable insights into its damping characteristics. Rebound resilience is defined as the ratio of the energy applied for deformation E_{drop} to the energy returned E_{reb} during a single impact (Equation (4))[29]

$$R = \frac{E_{reb}}{E_{drop}} = \frac{h_{reb}}{h_{drop}} = \frac{{v_{reb}}^2}{{v_{drop}}^2} \quad (4)$$

To determine the rebound resilience for each blend, we conducted ball drop experiments using pretempered dampers, spanning temperatures from −50 to +50 °C. Examining silicone specimens within a defined temperature range is vital due to the substantial impact of temperature on both their mechanical properties and damping behavior. These ball drop experiments aiming at impact protection were performed at heights of 25, 45, and 65 cm, employing steel balls with 3 and 4 cm diameters. To minimize adhesion effects, blend test specimen's surfaces were treated with chalk.

Figure 4c illustrates the temperature dependency of rebound height for Sylgard 184 (A) and Ecoflex 00–30 (B) specimens. The rebound height increases with increasing temperature, corresponding to decreasing damping capabilities. This phenomenon can be attributed to the complex micromolecular structure characterized by interwoven molecular chains that move at more freedom at elevated temperatures. With increasing temperature, the elastic modulus of unfilled elastomers increases caused by the entropy–elasticity of macromolecules and, hence, the increased mobility of the molecules to resist the orientation of the macromolecules (i.e., reduction of entropy) to align with the direction of external loading. This effect is observed for unfilled silicone rubber and other elastomers like natural rubber. In silicone rubber, the glass transition temperature is very low (around −110 °C)[30] and at ambient temperatures the molecular chain mobility is leading to the observation of high mechanical flexibility, resilience and entropy–elasticity. **Figure 5a** shows the rebound resilience from the test involving the 3 cm ball dropped from a 45 cm height at 30 °C. The obtained data confirm the trend in damping properties already observed when calculating dissipated energy as previously summarized in Table 1. Pure Ecoflex 00–30 (E100) and Sylgard 184 (E0) specimen exhibit the lowest and the second lowest rebound resilience corresponding to best damping performance, while the least effective damping behavior was observed at a 60 wt% Ecoflex 00–30 (E60) content. The 50, 70, and 80 wt% Ecoflex 00–30 (E50, E70, and E80) blends only show marginal better damping, visible from a zoomed in graph in Figure S3 (Supporting Information). They are closely followed by E40 and E90. E30 and E20 perform better with E10 being the best aside from the pure E100 and E0. This trend persists across the entire temperature range, with lower temperatures resulting in reduced rebound resilience and, consequently, increased damping capacity. Notably, for high concentrations of Ecoflex 00–30, there is a sudden increase in rebound resilience at around −30 °C, significantly higher than the glass transition temperature and therefore attributed most likely to a phase transition such as melting.[31,32] Further details on the influence of ball dimensions and height can be found in Figure S4 (Supporting Information).

As viscoelasticity in silicones is inherently velocity dependent, we explored the influence of height and impact velocity on dissipative behavior by comparing rebound resilience at various dropping heights. The results, shown in Figure 5b, display the average rebound resilience across different drop heights. Dashed lines denote the lower and upper limits, representing the maximum

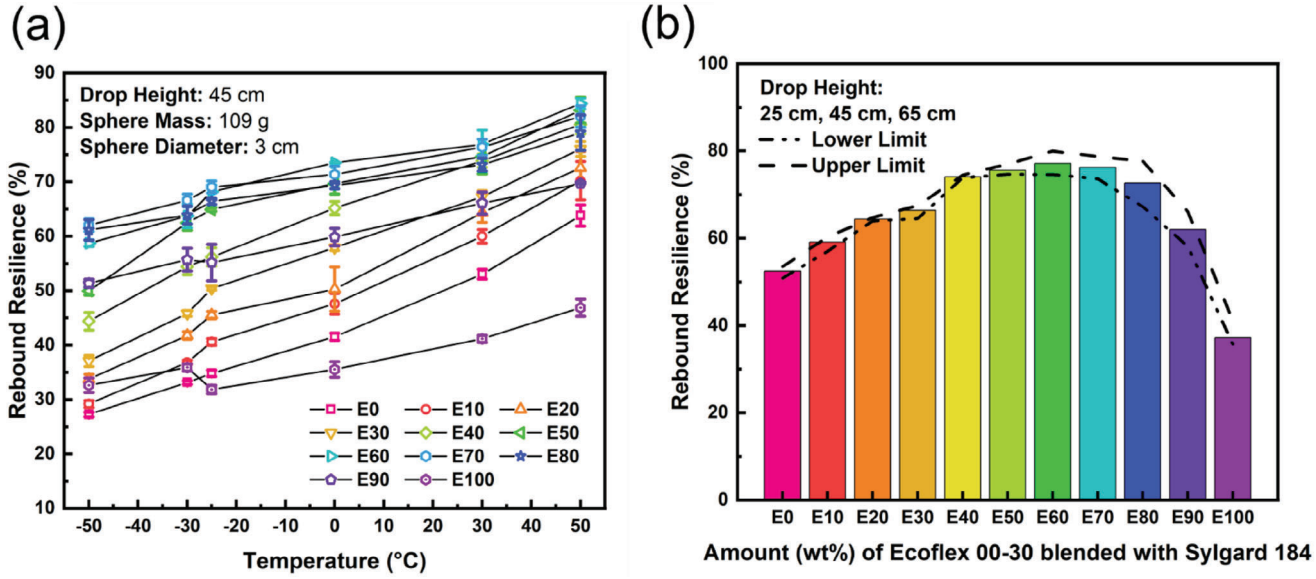

Figure 5. a) Rebound resilience as a function of temperature for Ecoflex 00–30 (E100), Sylgard 184 (E0), and their blends. The experiment involves a 3 cm diameter ball released from a height of 45 cm. b) The arithmetic mean of rebound resilience, averaged across various drop heights (25, 45, and 65 cm), for the 3 cm stainless-steel ball impacting elastomer blends. The dashed lines indicate the upper and lower limits, representing the maximum and minimum values and highlighting variations in dissipation with dropping height.

and minimum rebound heights. While the results reveal a subtle height dependency, the overall trend indicates minimal change, with a deviation of 1% for Sylgard 184 (E0) and 3% for Ecoflex 00–30 (E100). Blending introduces a more pronounced time-dependent aspect, especially notable at higher concentrations of Ecoflex 00–30, with the most significant deviation being ≈4%. Consequently, both Ecoflex 00–30 and Sylgard 184 not only exhibit superior damping characteristics but also demonstrate negligible velocity dependency compared to their blends. To highlight the comparability of our ball drop test, we also conducted pendulum impact tests (Figure S5, Supporting Information) that show good agreement with data derived from tracking (Figure 2c) and rebound resilience (Figure 5a).

The ball drop experiment, in general, and the rebound resilience, in particular, can be analyzed as two distinct phases: first, the energy recovered (observable in the rebound height) referred to as E' and second, the energy lost during impact due to factors such as friction and internal motion, described as E''. This process mirrors the principles observed in DTMA, where materials are characterized by storage and loss moduli.[33] Returning to the analogy of the ball resembling a spherical indenter, we can once more leverage this concept of an impact experiment to explore the dynamic behavior of the elastomeric material, as previously applied in the field of materials science.[34,35]

When analyzing the dynamic interaction between an impacting sphere and a soft elastomer during contact, we conceptualize the system as a vibrating mechanical system. To describe the mechanical behavior of the test specimen in this context, we apply the Kelvin–Voigt model (Equation (5)),[36] consisting of a parallel spring (characterized by the spring constant k) and a dashpot (characterized by the damping coefficient c) and the free decay oscillation model (Equation (6)) as well as the log of height approximation (Equation (7)), proposed by Chen and Lakes.[37] These models allow establishing a theoretical relationship between the rebound resilience and the velocity terms before and after the impact, expressed as

$$R = \left[\frac{\dot{x}_t}{\dot{x}_0}\right]^2 = \exp\left[-2\frac{1-\sqrt{1-\tan\delta^2}}{\tan\delta}\left(\pi - \sin^{-1}\tan\delta\right)\right] \tag{5}$$

$$R = \left(\cos\delta + \tan\frac{\delta}{2}\sin\delta\right)\mathrm{e}^{-2\tan(\delta/2)(\pi-\delta)} \tag{6}$$

$$\tan\delta \cong \frac{\ln\left(\left(\frac{\dot{x}_t}{\dot{x}_0}\right)^2\right)}{\pi} \tag{7}$$

Here, R represents the rebound resilience, $\dot{x}_0$ and $\dot{x}_t$ are the velocities before and after the contact, and tanδ denotes the loss tangent. A visual representation of this relationship is provided in **Figure 6a**.

Hardness of elastomers, specifically rubbers, correlates with the Young's modulus as experimental impact studies showed.[38] According to classical elastic theory,[2] there is a firmly established correlation among the applied force F, Young's modulus E, radius of indenter r, and the indentation depth d.[39] This relation was later adapted to describe the indentation of elastomers[38] and is as follows

$$F = aEr^2\left(\frac{d}{r}\right)^n \tag{8}$$

where a and n are constants.

Later this relationship (equation 8) was found to be valid for dynamic measurements and was adapted to characterize the

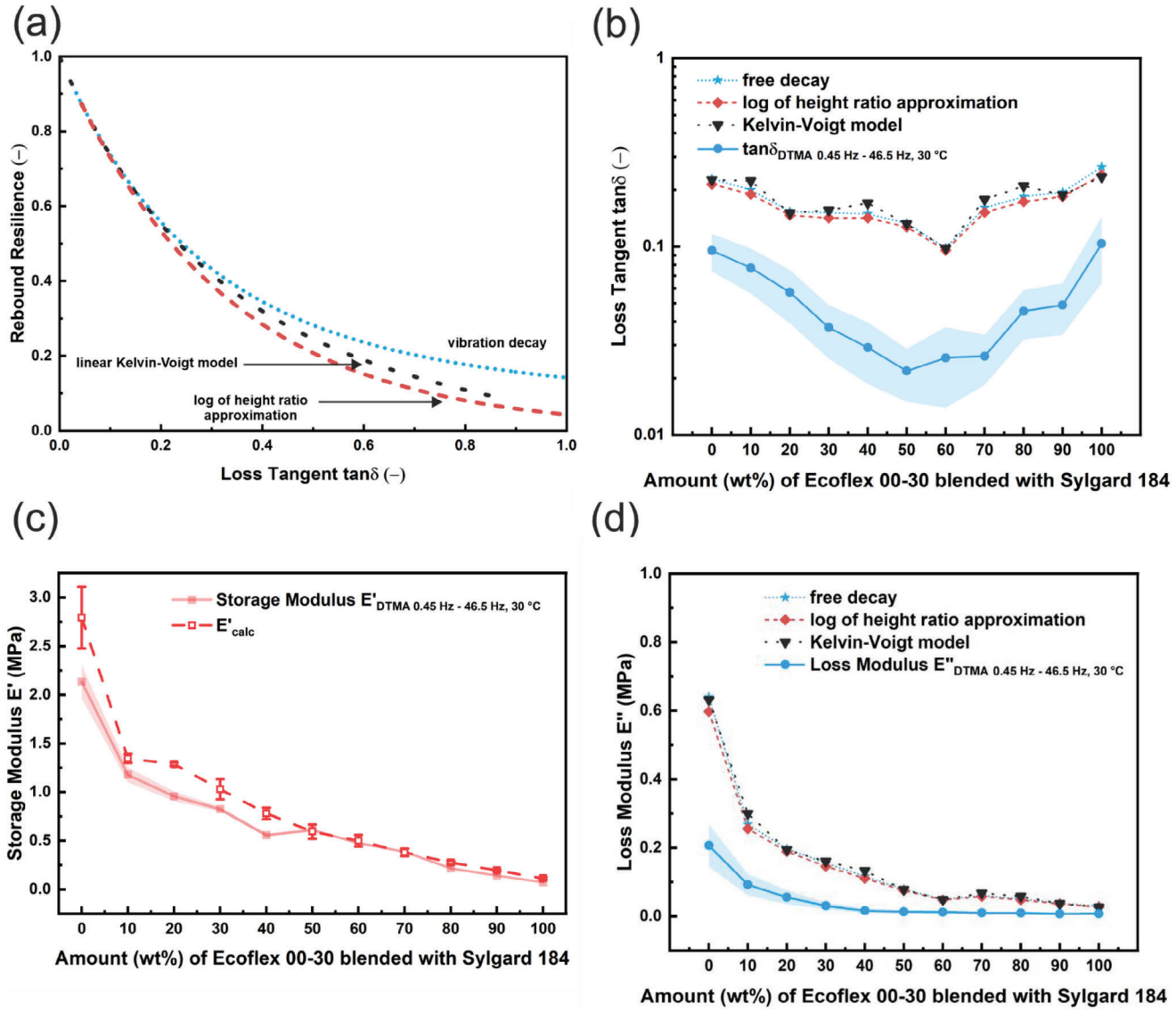

Figure 6. a) Various theoretical models for correlation of rebound resilience and loss tangent. b) Loss tangent calculated using different models (dashed lines) alongside the corresponding measured loss tangent (blue line). Data obtained through dynamic thermomechanical analysis across frequencies ranging from 0.45 to 46.5 Hz. c) Calculated dynamic storage modulus (dashed red line) and the corresponding data (0.45 Hz – 46.5 Hz) from DTMA measurements. d) Comparison of loss moduli calculated with various models (dashed lines) against the measured loss modulus (blue line) obtained through dynamic thermomechanical analysis across frequencies from 0.45 to 46.5 Hz.

storage modulus E' of elastomers[36]

$$E' = \frac{M\ddot{x}_{max}}{ar^2}\left(\frac{r}{x_{max}}\right)^n \tag{9}$$

where M and $\ddot{x}_{max}$ represent the mass of the indenter and the maximum acceleration, respectively, E' denotes the storage modulus, r is the radius of the indenter tip, x_{max} is the maximum depth of indentation, and $a = 1.98$ and $n = 1.48$ are constants.[38]

The loss modulus, E'', is determined by the equation

$$E'' = E' \tan\delta \tag{10}$$

where values for tan δ are obtained from Equations (5)–(7).

We calculated the storage modulus, loss modulus, and the loss tangent for all the blends using displacement and acceleration data acquired from the ball drop experiment, which utilized a sphere with a diameter of 2 cm, dropped from a height of 45 cm onto specimens tempered at +30 °C.

Furthermore, to validate the experimental results, DTMA measurements were performed over a frequency range spanning from 0.45 to 46.5 Hz and at temperatures ranging from −50 to +50 °C. For further information on DTMA datasets, refer to Figure S1 (Supporting Information).

Subsequently, the calculated and experimental results for the loss tangent tan δ at +30 °C are showcased in Figure 6b. Derived from rebound resilience data and employing diverse models (see Equations (5)–(7)), the calculated values for the loss tangent

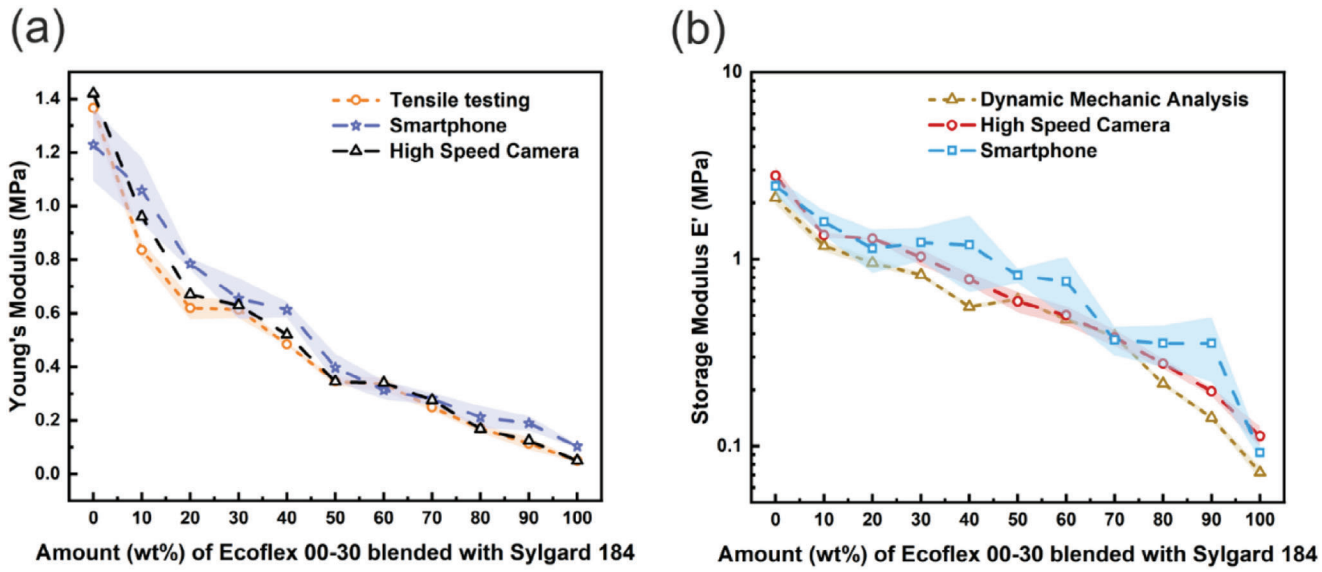

Figure 7. The results of a) Young's modulus and b) storage modulus obtained from video recordings using a Samsung Galaxy Note S10 Plus smartphone's slow-motion feature. The data were analyzed via the Kelvin–Voigt model and demonstrated a high degree of alignment with the results of high-speed cameras, tensile tests and DTMA.

exhibited a fourfold deviation compared to the experimentally determined values. This underscores the need to refine and adjust the theoretical models to better align with empirical observations. A possible approach is the use of viscoelastic constitutive models developed in a continuum mechanics framework as an alternative to computing a single value for the loss tangent. By developing such a viscoelastic model using a Prony series representation of storage and loss moduli, and applying it in a large-strain regime,[40] the experimental conditions of the ball drop test should be better matched. Furthermore, it is imperative to acknowledge the frequency dependency, which manifests as an increase in tan δ observed in DTMA measurements. This necessitates further investigations into the vibrational state of the testing specimen upon impact.

In conjunction with the analysis of the loss tangent, we investigated the storage modulus using the linear Kelvin–Voigt model. Equation (9) was applied to compute the storage modulus for the testing specimens, utilizing acceleration and indentation depth data from tracking. Notably, Figure 6c demonstrates a robust agreement between the calculated storage modulus values and the experimental data. Both consistently depict a decrease as the content of Ecoflex 00–30 increases. For a comparison of the experimental values with the calculated values, please refer to Table S2 (Supporting Information).

For comprehensive analysis, we calculated the loss modulus for the diverse testing specimens using Equation (10) (refer to Figure 6d). Much like the loss tangent, the loss modulus exhibits a significant deviation compared to the DTMA data, highlighting the need for an improved theoretical model to establish a better correlation between rebound resilience and loss tangent. Despite the alignment observed in the calculated storage modulus with experimental data, an adapted theoretical model holds the potential to offer deeper insights into the complete dynamic mechanical behavior of the testing specimen, providing a more comprehensive understanding of its dissipative characteristics. Overall, the data indicate that determining the dynamic properties through a ball drop experiment by adjusting the underlying theory of the material modeling should be feasible.

The whole idea of conducting the ball drop experiments was providing an alternative method for evaluating the mechanical properties of silicone elastomer materials in any lab. Our main emphasis was on achieving a procedure that combines simplicity and cost-effectiveness to make it accessible to everyone. Traditionally, such experiments require the use of a high-speed camera, which is quite costly. To address the cost constraint, we additionally conducted the ball drop experiment using a smartphone. The smartphone selection criteria were straightforward, focusing on the capability to capture videos at high frame rates. The Samsung Galaxy Note S10 Plus was selected due to its built-in Super-Slow-motion feature, allowing video recording at 960 fps with a resolution of 1280 × 720 pixels. This choice resulted in an experimental setup with a total cost of under 500 Euros, making it accessible to a very broad range of users. **Figure 7** summarizes the results of the ball drop experiment recorded with the selected smartphone.

The experiments were conducted on the previously described silicone blends of Ecoflex 00–30 and Sylgard 184, pretempered at 30 °C, with a drop height of 25 cm and a sphere size of 2 cm. The impact event was captured using the smartphone and subsequently processed and analyzed using Tracker software. In Figure 7a, the values calculated using the Kelvin–Voigt model for the Young's modulus of the Ecoflex 00–30, Sylgard 184 and their blends, derived from both smartphone and high-speed camera data, are compared to the conventional tensile testing results presented earlier in Figure 3a. To our delight, the results obtained from the smartphone recordings are in good agreement with both the high-speed camera and tensile test data. A minor discrepancy in the data is noticeable, attributed to the lower frame rate captured during the impact, resulting in a smaller dataset for the evaluation process. In addition to the elastic modulus, we

also determined the storage modulus using data captured by the smartphone, as illustrated in Figure 7b. While the results again demonstrate a good agreement with DTMA data and high-speed camera data, the results reveal a significant deviation due to the constraints in available data points. Given that the calculation process relies heavily on both the indentation depth and the acceleration data (the second derivative of the sphere's trajectory), the latter proves somewhat imprecise due to limitations in frame rate. Despite the challenges, this shows that a determination of both the Young's modulus and the complex moduli such as the storage modulus is possible. Furthermore, this provides a cheap and simple means for researchers worldwide for characterizing material properties in silicone elastomers without the need of expensive and complicated equipment.

3. Conclusion

Our aim was to develop an affordable ball drop test setup for characterizing soft materials with a focus on damping, emphasizing simplicity and practicality. The conceived setup, consisting of an aluminum frame, ball release mechanism, and a high-speed camera, was employed to investigate the influence of blending elastomers (polydimethylsiloxanes) with different shore hardness on mechanical properties under diverse conditions. This setup allows for the adjustment of drop height and the use of pretempered specimens to analyze viscoelastic behavior, including velocity dependency across a broad temperature range. The ball's impact trajectory was analyzed, and vital material parameters such as Young's modulus, dissipated energy, rebound resilience, storage modulus, loss modulus, and the loss tangent of the elastomer blends were extracted utilizing high-speed monitoring and free software like Tracker by Physlet. We showed the influence of experimental conditions such as drop height, sphere diameter, and temperature to provide a bigger picture of the method. Additionally, we compared to traditional setups such as DTMA and methodologies with similar design such as a pendulum test. Limitations are clearly due to the inability to provide frequency-dependent data as well as the requirement for carefully selecting test specimen's dimensions in relation to those of the balls.

In summary, our findings closely correspond with experimental data obtained through traditional, however, often costlier, techniques such as the tensile test and dynamic thermomechanical analysis in materials science, particularly in relation to Young's modulus and storage modulus. Moreover, the development of an adapted theoretical model becomes imperative to address the fourfold shift observed in the calculated loss tangent using rebound resilience data.[40] This is crucial for advancing the potential of ball drop testing as an alternative method for material testing in future applications. Additionally, our cost-effective approach, employing a mid-budget smartphone to capture impact events, offers researcher worldwide, in particular physicists and chemists,[41] an accessible method for material characterization. Our innovative ball drop test and the accompanying data evaluation opens up new avenues for characterizing soft materials, providing a budget-friendly solution with versatile applications. We therefore hope this approach provides new impulses for simple material characterization based on basic physic concepts.

4. Experimental Section

Preparation of Sylgard 184 and Ecoflex 00–30 and Elastomer Blend Samples for Ball Drop Experiments: Ecoflex 00–30 and Sylgard 184 were prepared according to the manufacturer's instructions, Sylgard 184 (DowSil) 10:1 and Ecoflex 00–30 (Smooth-On) 1:1. They were weighted in 125 mL polypropylene beakers, and afterward mixed to the specific mixing ratio by weight. The samples were mixed using a bladeless mixer (Hauschild Speedmixer DAC 400) for 1 min (40 s at 600 rpm and 20 s at 1000 rpm) and then degassed in a desiccator to remove air bubbles. The blends were created by initially preparing both base materials, Ecoflex 00–30 and Sylgard 184, followed by the addition (depending on the mixing ratio) of a specific weight percentage of Sylgard 184 to Ecoflex 00–30. Subsequently, the blends underwent mixing in a bladeless mixer for 1 min (40 s at 600 rpm and 20 s at 1000 rpm), followed by an additional degassing step. The degassed elastomer was filled in a poly(methyl metacrylate) (PMMA) mold, fabricated by laser cutting (Trotec Speedy 300), specifically designed to fabricate cylindrical samples with a diameter of 6 cm and a height of 2 cm, followed by a second degassing step. The molds were then put into the oven and cured for 24 h at a temperature of 65 °C. This ensured well-cured samples with minimal changes due to further crosslinking/curing as to be expected for lower and shorter curing temperatures. After dismantling the molds, excessive elastomer, owed to fabrication, was carefully removed with scissors, providing cylindrical-shaped samples. Finally, the samples were chalked to minimize adhesion.

Preparation of Sylgard 184 and Ecoflex 00–30 and Elastomer Blend Samples for Tensile Testing and Dynamic Thermomechanical Analysis: The testing specimens were prepared as 3D dumbbell-shaped specimens (dimensions and drawing can be found in Figure S6 in the Supporting Information). Moreover, a mold, made of Teflon was used to provide easy removability of the elastomer dumbbell-shaped specimen. First, the elastomers were prepared according to the manufacturer's instructions, Sylgard 184 (10:1) and Ecoflex 00–30 (1:1), by weighting it in a polypropylene beaker and subsequently mixing in a bladeless mixer (Hauschild Speedmixer 400). Afterward, blending was done by adding Sylgard 184 to Ecoflex 00–30 by weight, depending on the desired mixing ratio. The blends were again mixed using a bladeless mixer and afterward poured into the mold. Finally, the samples were degassed in a desiccator to remove air bubbles and then put in an oven for 24 h at 65 °C. After that, the molds were dismantled and specimens were ready to test.

Ball Drop Experiment: In setting up the ball drop experiment, a framework comprising a release mechanism for securely holding and subsequently releasing the sphere, a ruler for postprocessing video analysis reference, the test specimens, and a high-speed camera capable of recording at elevated frame rates was assembled. Steel balls (made of X46Cr13) ranging from 1 to 4 cm in diameter were dropped from heights of 25, 45, and 65 cm onto cylindrical silicone elastomer blends with a consistent diameter of 6 cm and a height of 2 cm. To ensure consistency, these blends underwent preconditioning for 2 h in an environmental chamber, maintaining temperatures between −50 and +50 °C. The high-speed camera (Phantom v711-8G-M, ViSiON RESEARCH) recorded the ball drop experiments at a frame rate of 1600 with a resolutions of 1024 × 768 or 1024 × 800, respectively. Three distinct sets of measurements were conducted. The first set involved dropping spheres of sizes 3 and 4 cm from heights of 25, 45, and 65 cm onto Ecoflex 00–30 and Sylgard 184 as well as their blends preconditioned at temperatures ranging from −50 to +50 °C. This set aimed at evaluating damping characteristics through rebound resilience and energy dissipation within the hysteresis area. The second set focused on silicones preconditioned at +30 °C, with spheres ranging from 1 to 4 cm in diameter dropped from a height of 45 cm. This set provided data for determining Young's modulus and complex moduli. The third set, conducted 6 months after the initial measurements, involved dropping a 2 cm sphere from a height of 25 cm onto +30 °C preconditioned silicones. Notably, this experiment was recorded using a smartphone (Samsung Galaxy Note S10 Plus) instead of a high-speed camera, offering a frame rate of 960 and a resolution of 1280 × 720. The video footage served as the basis for comparing data obtained from both the smartphone and the high-speed camera. Subsequently, the video recordings underwent postprocessing using

open-source software Tracker (Physlets). All presented data points were averaged over three samples with three experiments each in total, adding up to nine experiments for each data point.

Video Recording, Postprocessing, and Analysis: For controlling the high-speed camera (Phantom v711-8G-M, Vision Research), the Phantom Camera Software (PCC v3.8) was utilized. The camera settings were configured to capture at 1600 fps with resolutions of 1200 × 800 and 1024 × 768 for the first and second sets of measurements, respectively. The exposure (µs) was set to 330 and 200 for the first and second sets, enabling a recording time of ≈4000 individual frames, covering the entire sequence from drop to rebound. Upon recording, the saved cine files were converted to the mp4 file format to facilitate postprocessing through the open-source Tracker software (Physlets). Recordings made using the smartphone's super-slow-motion feature were inherently in the mp4 format. It is worth noting that next-generation smartphones no longer capture high frame rates, instead employing interpolation techniques for recording. This influenced the choice of the Samsung Galaxy Note S10 Plus, offering a native 960 frames with a 0.2 s time window for video capture. Subsequently, both the converted cine files and smartphone recordings were imported into the Tracker software. The software settings were adjusted to match the frame rate of the videos, ensuring accurate calculation of velocity and acceleration. The ruler visible in the video provided a reference for converting pixels to length, and the software allowed for verification of the sphere's size using the ruler tool. The coordinate system was established at the upper surface of the visible specimen, serving as the origin of the coordinate system. A point mass was assigned to the upper part of the sphere, later corrected to the lower part by subtracting the sphere's size during evaluation in OriginLab software. Autotracking was initiated, tracing the point mass in each frame and yielding information on trajectory, velocity, and acceleration. These data were then exported as a txt-file and analyzed in Origin.

Supporting Information

Supporting Information is available from the Wiley Online Library or from the author.

Acknowledgements

The financial support by the Austrian Federal Ministry for Digital and Economic Affairs, the National Foundation for Research, Technology and Development, and the Christian Doppler Research Association is gratefully acknowledged. Open Access Funding by the University of Linz.

Conflict of Interest

The authors declare no conflict of interest.

Data Availability Statement

The data that support the findings of this study are available from the corresponding author upon reasonable request.

Keywords

ball drop experiment, damping, dissipation, elastomer blends, elastomers

Received: March 20, 2024
Revised: May 10, 2024
Published online: June 25, 2024

[1] R. Cross, *Phys. Educ.* **2015**, *50*, 335.
[2] H. Hertz, *J. Reine Angew. Math* **1881**, *92*, 156.
[3] K. L. Johnson, *Proc. Inst. Mech. Eng.* **1982**, *196*, 363.
[4] S. Li, J. Zhang, J. He, W. Liu, Y. Wang, Z. Huang, H. Pang, Y. Chen, *Adv. Sci.* **2023**, *10*, 2304506.
[5] J. Y. Oh, Z. Bao, *Adv. Sci.* **2019**, *6*, 1900186.
[6] D. Qi, K. Zhang, G. Tian, B. Jiang, Y. Huang, *Adv. Mater.* **2021**, *33*, 2003155.
[7] A. Tan, L. Pellegrino, Z. Ahmad, J. T. Cabral, *Adv. Opt. Mater.* **2022**, *10*, 2200964.
[8] S. Bauer, S. Bauer-Gogonea, I. Graz, M. Kaltenbrunner, C. Keplinger, R. Schwödiauer, *Adv. Mater.* **2014**, *26*, 149.
[9] G. Whitesides, *Angew. Chem., Int. Ed.* **2018**, *57*, 4258.
[10] F. Schneider, T. Fellner, J. Wilde, U. Wallrabe, *J. Micromech. Microeng.* **2008**, *18*, 065008.
[11] R. Moser, G. Kettlgruber, C. M. Siket, M. Drack, I. M. Graz, U. Cakmak, Z. Major, M. Kaltenbrunner, S. Bauer, *Adv. Sci.* **2016**, *3*, 1500396.
[12] S. E. Schausberger, R. Kaltseis, M. Drack, U. D. Cakmak, Z. Major, S. Bauer, *IEEE Access* **2015**, *3*, 556.
[13] S. O'sullivan, R. Nagle, J. A. McEwen, V. Casey, *J. Phys. D: Appl. Phys.* **2003**, *36*, 1910.
[14] Z. Wang, A. A. Volinsky, N. D. Gallant, *J. Appl. Polym. Sci.* **2014**, *131*, 41384.
[15] M. Bont, C. Barry, S. Johnston, *Polym. Eng. Sci.* **2021**, *61*, 331.
[16] A. Yepremyan, A. Osamudiamen, M. A. Brook, A. Feinle, *Chem. Commun.* **2020**, *56*, 13555.
[17] C. Emminger, U. D. Çakmak, R. Preuer, I. Graz, Z. Major, *Materials* **2021**, *14*, 7639.
[18] A. Haron, K. A. Ismail, *IOP Conf. Ser.: Mater. Sci. Eng.* **2012**, *36*, 012038.
[19] J. Vaicekauskaite, P. Mazurek, S. Vudayagiri, A. L. Skov, *J. Mater. Chem. C* **2020**, *8*, 1273.
[20] C. W. de Silva, *Vibration Damping, Control, and Design*, CRC Press (Taylor & Francis Group), Vancouver, Canada **2007**.
[21] W. C. Oliver, G. M. Pharr, *J. Mater. Res.* **1992**, *7*, 1564.
[22] G. M. Pharr, W. C. Oliver, *MRS Bull.* **1992**, *17*, 28.
[23] K. Pompel, Stainless steel ball 1.4034 Datasheet, https://www.kugelpompel.at/img/cms/Datenbl%C3%A4tter%20NiroStahl/Data%20sheet%20stainless%20steel%20ball%201-4034%20V1-01.pdf, (accessed: February, **2024**).
[24] E. Stockburger, H. Wester, J. Uhe, K. Brunotte, B. A. Behrens, *Proc. of the 9th Congress of the German Academic Association for Production Technology (WGP)*,Springer, Berlin **2019**, pp. 159–168.
[25] A. Müller, M. C. Wapler, U. Wallrabe, *Soft Matter* **2019**, *15*, 779.
[26] B. Poon, D. Rittel, G. Ravichandran, *Int. J. Solids Struct.* **2008**, *45*, 6018.
[27] B. Poon, D. Rittel, G. Ravichandran, *Int. J. Solids Struct.* **2008**, *45*, 6399.
[28] L. G. Treloar, *The Physics of Rubber Elasticity*, Oxford University Press, Oxford **1975**.
[29] R. S. Lakes, *Viscoelastic Materials*, Cambridge University Press, Cambridge **2009**.
[30] N. Bosq, N. Guigo, J. Persello, N. Sbirrazzuoli, *Phys. Chem. Chem. Phys.* **2014**, *16*, 7830.
[31] Y. Fang, Y. Li, X. Wang, Z. Zhou, K. Zhang, J. Zhou, B. Hu, *Small* **2020**, *16*, 2000450.
[32] A. M. Stricher, R. G. Rinaldi, C. Barrès, F. Ganachaud, L. Chazeau, *RSC Adv.* **2015**, *5*, 53713.
[33] K. P. Menard, N. Menard, *Dynamic Mechanical Analysis*, CRC Press, Boca Raton, FL **2020**.
[34] N. M. Vriend, A. P. Kren, *Polym. Test.* **2004**, *23*, 369.
[35] A. Meram, *Polym. Test.* **2019**, *79*, 106013.

[36] A. C. Bassi, *Polym. Eng. Sci.* **1978**, *18*, 750.
[37] C. P. Chen, R. S. Lakes, *Int. J. Solids Struct.* **1990**, *26*, 1313.
[38] R. D. Stiehler, G. E. Decker, G. W. Bullman, *Rubber Chem. Technol.* **1979**, *52*, 255.
[39] S. Timoshenko, *Theory of Elasticity*, McGraw-Hill, New York **1951**.
[40] M. Kunzemann, L. K. Doppelbauer, R. Preuer, A. Pechstein, arXiv:2402.07555v1, **2024**.
[41] E. Ajvazi, F. Bauer, P. Strasser, O. Brüggemann, R. Preuer, M. Kracalik, S. Hild, M. Abbasi, I. Graz, I. Teasdale, *ACS Polym. Au* **2024**, *4*, 56.

